BIBECHANA
Vol. 23, No. 3, August 2026, 31-40

ISSN 2091-0762 (Print), 2382-5340 (Online)
Journal homepage: http://nepjol.info/index.php/BIBECHANA
Publisher:Dept. of Phys., Mahendra Morang A. M. Campus (Tribhuvan University)Biratnagar

Ageing variability in single-crystal NMC811 under mission-profile cycling: stochastic and diffusion-controlled insights

Saroj Khanal[1*], Diwas Parajuli[2], Arjun Bhattarai[2], Prakriti Bagale[2], Himesh K.C.[2], Apekshya Pandey[2], Sakshyam Duwadi[2], Bhabishya Sapkota[2]

[1]*Amrit Science Campus, Tribhuvan University, Kathmandu, Nepal.*
[2]*Sunrise English Secondary School, Chitwan, Nepal.*

[*]Corresponding author: Email: hamiduimatra@gmail.com

Abstract

Nominally identical nickel-rich NMC811 cathodes do not age in the same way. Even under identical cycling conditions, capacity trajectories diverge over time. Three cells from a fork-lift mission-profile dataset were analyzed. Results were compared with a larger fast-charging dataset containing 46 commercial lithium-ion cells. Capacity fade was evaluated round by round, and variability was quantified using the coefficient of variation (CV%) and an early-cycle deviation metric. Cycling caused variability in both datasets to rise from less than 1% CV to more than 3%. A diffusion-limited square-root ageing model was used to represent transport-controlled ageing. The model produces smoother capacity trends and a modest reduction in variability, but cell–to–cell differences persist. Early–stage heterogeneity remains linked to long-term divergence. Al_2O_3 coatings can promote diffusion-limited behaviour, while the model used here represents this regime conceptually rather than a specific coating system. The results point to a two–stage ageing pattern, with early divergence followed by partial moderation under transport influence.

Keywords
Stochastic degradation, early–cycle deviation, diffusion–limited aging, capacity decline, NMC811 cathodes.

Article information
Manuscript received: April 28, 2026; Revised: June 28, 2026; Accepted: June 29, 2026
DOI: https://doi.org/10.3126/bibechana.v23i3.93542

1 Introduction

Lithium–ion batteries have become essential for electric vehicles, grid storage, and portable electronics because of their high energy density and long cycle life. Improving battery durability remains a major challenge, particularly for high-energy-density cathode materials. Among these, nickel–rich layered oxides such as NMC811 ($LiNi_{0.8}Mn_{0.1}Co_{0.1}O_2$) have attracted significant

interest because they offer high capacity while reducing cobalt content.

Ni–rich cathodes undergo chemo-mechanical and interfacial degradation processes, including anisotropic lattice changes, phase transitions, and surface reconstruction driven by electrolyte reactivity, during repeated lithiation and delithiation [1–4]. Increased nickel content seems to be consistent with the loss of structural and interfacial stabilities, thus resulting in an enhanced degradation rate in the surface and bulk regions. In order to increase the capacity of such batteries, it is suggested to increase the Ni content in layered cathode materials, for which NMC811 has widely been used [5,6]. Other processes, such as cathode-electrolyte interphase evolution and transition-metal dissolution, contribute to capacity fade and impedance growth, which becomes noticeable at high voltage and under fast charging conditions [7–9].

However, degradation does not occur uniformly across all cells, which results in measurable cell–to–cell variability even under nominally identical conditions. Single–crystal NMC811 reduces intergranular cracking but does not eliminate other degradation mechanisms. Surface reactions persist, intra–particle stress remains, and reaction kinetics can vary within individual particles [8,10]. Surface coatings, such as Al_2O_3 applied by atomic layer deposition (ALD), have been widely investigated to improve cathode stability by limiting interfacial reactions [11, 12]. Small differences during early cycling influence later ageing behaviour, with divergence between cells increasing over time [13,14]. The evolution of this variability and its relationship to long-term performance are not yet clearly quantified.

Existing literature has mainly focused on degradation mechanisms and strategies to improve average battery performance. In contrast, the evolution of cell-to-cell variability during cycling has received less attention. It is unclear whether early deviations between cells are linked to long-term performance differences. Reported performance improvements depend strongly on operating conditions. However, the effect of such coatings on cell-to-cell variability remains less clearly understood [10, 15]. In particular, it is not well established whether coatings reduce variability across cells or primarily shift overall degradation rates. In this study, ageing variability was analyzed using two datasets: a mission–profile dataset from Vilsen and Stroe [14], and the analysis was extended using the subset of the Massachusetts Institute of Technology (MIT) fast-charging Severson dataset [16]. The coefficient of variation (CV%) was used to quantify dispersion, and an early–cycle deviation metric was introduced to examine the relationship between initial differences and long-term capacity. A simplified diffusion-limited, transport–controlled ageing model was developed to study cell performance during ageing.

2 Theoretical framework

Two limiting physical regimes are considered for interpreting ageing in single–crystal NMC811 cathodes. One regime assumes reaction control with spatially heterogeneous degradation. The other assumes diffusion control, where transport kinetics limit the ageing rate. Electrochemical kinetics, statistical fracture theory, and diffusion transport each provide partial grounding for these regimes. No single theory suffices. The framework adopted here is therefore minimal. It serves two purposes only: first, to interpret how variability evolves during cycling; second, to support the model–based comparison presented in Section 4.

2.1 Reaction-limited stochastic ageing in uncoated SC-NMC811

For uncoated single–crystal NMC811, localized electrochemical reactions at heterogeneous active sites drive degradation. Take a representative domain i. The local reaction rate, following an Arrhenius expression, includes electrochemical driving forces and can be expressed as [2,5,8]

$$r_i = A_i \exp \frac{-E_a}{RT} f(Ni^{4+})\eta_i \tag{1}$$

where r_i is the reaction rate, A_i the pre-exponential factor, E_a the activation energy, $f(Ni^{4+})$ the fraction of high-valence Ni sites, and η_i the local overpotential [2,5,8].

Microcrack initiation and propagation represent a probabilistic form of mechanical degradation. Weibull statistics offer a natural description. The distribution has seen wide use in fracture mechanics, expressed as [17]

$$P_{crack}(x) = 1 - \exp[-(\frac{x}{\lambda})^k] \tag{2}$$

where P_{crack} is crack probability, x represents stress or strain, and λ and k are Weibull scale and shape parameters respectively [17]. Heterogeneous reaction kinetics and probabilistic fracture behaviour do not act independently. Their combination yields degradation trajectories that vary across domains and also across cells.

2.2 Diffusion-limited ageing in Al_2O_3 coated SC-NMC811

Al_2O_3 coatings change the picture. Transport limitations, not localized reaction hotspots, now control degradation. Within the coating or the interfacial region, reactive species concentration evolves according to Fick's second law, given as [1, 10, 11]

$$\frac{\partial C}{\partial t} = D\frac{\partial^2}{\partial x^2} \tag{3}$$

where C is reactive species concentration, t is time, and D is effective diffusivity. Equation (3) captures diffusion-controlled transport across interfacial layers and coatings. Several studies of coated cathode systems support this interpretation [1,10,11]. When diffusion limits the ageing process, parabolic kinetics typically emerge. One consequence is a square-root dependence of capacity fade on time, expressed as [1, 8, 11, 18]

$$\Delta Q(t) \propto \sqrt{t} \tag{4}$$

Diffusion–controlled growth of interfacial layers, together with transport–limited reaction processes, causes this scaling. Both suppress localized hotspots and promote more uniform degradation. Diffusion-dominated ageing, therefore, imposes a spatial averaging effect. Variability across cells diminishes but never fully disappears.

2.3 Ageing regime and heterogeneity

Electrochemical rate theory supports that, in the reaction-limited regimes, Arrhenius kinetics (Equation (1)) create strong spatial variability. The reason is exponential sensitivity–to both activation energy and local over-potential [2, 5, 19]. Probabilistic fracture behaviour (Weibull distribution, Equation (2)) adds another layer. Defect–driven failure in brittle solids commonly uses this distribution [17]. Initial heterogeneities are amplified by the kinetics and fractures, which yield divergence across trajectories.

In diffusion-limited regimes, transport follows Fick's second law (Equation (3)), with flux driven by chemical potential gradients, $J = -\frac{D}{RT}C\nabla_\mu$, reflecting the tendency toward free–energy minimization [20, 21]. Equation (4) describes parabolic degradation kinetics which are typical for diffusion-controlled processes and interfacial growth [1, 11, 22].

Diffusion not only imposes spatial averaging but also tempers heterogeneity. However, heterogeneity is never fully removed. In fact, variability depends on which ageing regime dominates; reaction-limited processes amplify local differences, whereas diffusion-limited processes reduce them.

3 Data and methods

3.1 Dataset and processing

A publicly available battery degradation dataset from Vilsen and Stroe (2023/2024) was analyzed. The dataset comprises high-resolution operational and diagnostic data for commercial cells. The cycling protocol follows a realistic forklift duty profile [14]. The dataset contains three nominally identical cells, labeled Cells [1–3]. These cells were selected to assess cell-to-cell variability under identical operating conditions.

For each ageing round, two data files were used. The Ageing.csv file contained time–resolved operational data, while RPT.csv (Reference Performance Test) provided controlled measurements used for capacity evaluation. Thermal behaviour is interpreted in relation to peak temperatures reported in the dataset, which are known to correlate with accelerated degradation processes such as electrolyte decomposition and interfacial reactions [2, 5, 9].

Discharge capacity for each cell and each ageing round came from numerical integration of current over the discharge interval in RPT.csv [20]

$$Q(r) = \int_{t_0}^{t_{\text{end}}} I(t)\, dt \tag{5}$$

where $Q(r)$ is the capacity at round r and $I(t)$ is the instantaneous current.

3.2 Variability metrics

Cell–to–cell dispersion in capacity was quantified using the coefficient of variation (CV%) across cells for each ageing round

$$CV(r) = \frac{\sigma_Q(r)}{\mu_Q(r)} \times 100 \tag{6}$$

where $\sigma_Q(r)$ and $\mu_Q(r)$ are the standard deviation and mean capacity at round (r). Because CV% normalizes variability against absolute capacity, comparisons across different ageing stages and datasets become possible [9, 13].

We also wanted to know whether early-stage variability predicts later performance. So, we defined an early–cycle deviation metric. For each cell i, the deviation from the ensemble mean was calculated

using the first N ageing rounds. The metric is defined as follows

$$D_i = \frac{1}{N}\sum_{r=1}^{N} |Q_i(r) - \mu_Q(r)| \tag{7}$$

where $Q_i(r)$ is the capacity of the cell i at round r, and $\mu_Q(r)$ is the mean capacity across all cells at that round. This metric quantifies the magnitude of early–cycle divergence relative to the ensemble average and was subsequently compared with long-term capacity outcomes. Specifically, the relationship between D_i and final capacity $Q_i(r_{final})$ was examined.

3.3 Model and cross-dataset validation

Only uncoated cells appear in the primary dataset. To represent a coating-inspired ageing trajectory, we therefore fit a simplified diffusion-limited reference model to the experimental capacity data. For diffusion-controlled conditions, capacity evolution takes the following form [1, 8, 10, 11]

$$Q_{model}(r) = Q_0 - k\sqrt{r} \tag{8}$$

where Q_0 and k were determined by least–squares fitting for each cell. We compared the CV% from experimental data against the CV% from the fitted model. That comparison gave an estimate of the apparent reduction. The model itself serves only as a conceptual benchmark. It does not quantitatively predict how coated cells perform [1, 8, 10, 11]. We also wanted to know whether the observed trends hold more generally. So we extended the same analysis to the Severson et al. in 2019 MIT fast-charging dataset. That dataset includes 46 cells cycled under fast–charging conditions. Both datasets were analyzed using capacity, CV%, and the early–cycle deviation metric D_i.

3.4 Capacity scaling in the forklift dataset

Discharge capacity was obtained by integrating current from the RPT data (Equation (5)). The calculated capacities exceeded typical nominal values reported for similar cells.

Consistency was checked using the relation between energy, voltage, and capacity [14]

$$Q_{ref} = \frac{E}{V_{avg}} \tag{9}$$

The ratio between integrated and energy-derived capacity is [14]

$$S = \frac{Q_{int}}{Q_{ref}} = \frac{Q_{int} \times V_{avg}}{E} \tag{10}$$

The ratio remains close to unity across cells and ageing rounds.

3.5 Scope and limitations

The primary dataset consists of only three cells, and hence we acknowledge statistical generalization of results is limited. It is difficult to capture scale variability in such a small sample [14]. Adding the Severson dataset offers broader validation, but direct comparison faces a complication: cycling protocols and operating conditions differ between datasets. We also acknowledge our diffusion-limited model is simplistic, and it does not account for interfacial resistance growth, nor does it include mechanical degradation or temperature-dependent kinetics. The early-cycle deviation metric captures relative divergence well, but specific mechanistic contributions to degradation lie beyond its scope.

4 Results and discussion

4.1 Thermal behavior

Maximum cell temperature varied across the three nominally identical cells under identical cycling conditions [14]. Cells 2 and 3 maintained relatively stable thermal behaviour throughout cycling and did not exhibit significant temperature excursions. In contrast, Cell 1 experienced a pronounced temperature increase above 73°C during Rounds 50–55, indicating the onset of abnormal thermal behaviour that may be associated with accelerated degradation processes and increased heat generation within the cell, Figure 1. Such thermal instability may contribute to the irregular capacity decline observed at later stages of ageing and highlights the emergence of cell-to-cell variability despite nominally identical operating conditions. Elevated temperatures are linked to increased degradation rates and parasitic reactions [5, 9]. Cell 1 shows a temperature excursion together with irregular capacity behaviour. Localized degradation and heterogeneous ageing pathways have been reported for Ni-rich cathodes [8]. This behaviour follows the reaction-limited ageing framework described in Section 2. The divergence between cells points to stochastic ageing and is discussed further in the next section.

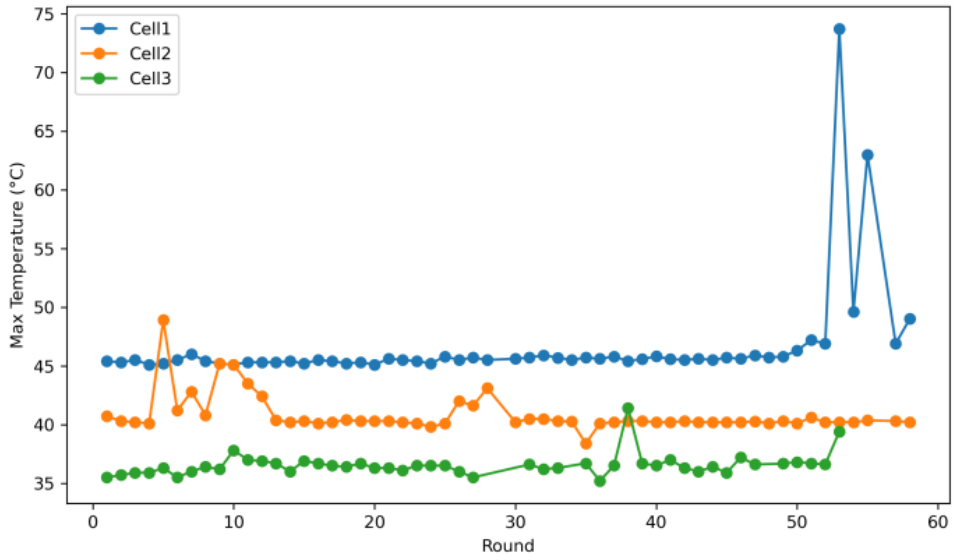

Figure 1: Discharge capacity and temperature for three cells from the Vilsen and Stroe (2024) dataset. Cell 1 shows a late–stage temperature excursion with an irregular capacity trajectory.

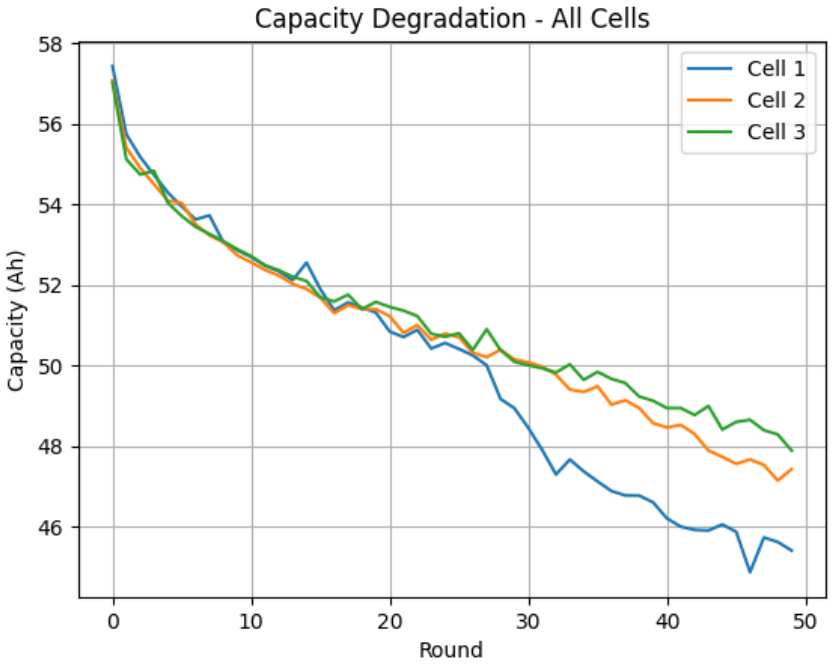

Figure 2: Discharge capacity across ageing rounds for three cells cycled under identical conditions. The three curves overlap during early cycles. Separation begins around mid-life, and Cell 1 subsequently shows a more pronounced decline.

4.2 Capacity divergence

Discharge capacity from RPT measurements declines with ageing round (Figure 2). All three cells show similar behaviour during early cycles, but their trajectories separate around mid-life. By Round 30, Cell 1 drops below the other two, while Cells 2 and 3 remain closely grouped. Cell 1 shows small irregular drops at later stages, while Cells 2 and 3 follow smoother trends. This matches the thermal behaviour in Figure 1, where only Cell 1 shows a late-stage temperature rise. Capacity values were obtained from integrated current data. Energy–voltage checks confirm agreement between current, voltage, and energy measurements, with no additional correction required. A transition from

similar early behaviour to diverging ageing trajectories is observed. Ni-rich cathodes show similar behaviour, where local variations in reaction kinetics and microstructure contribute to non-uniform degradation [8, 13].

The onset of separation around mid-life suggests that initially small cell–to–cell differences become amplified with continued cycling. During the early ageing stage, degradation proceeds relatively uniformly across the three cells, resulting in similar capacity trajectories. As cycling progresses, cumulative differences in interfacial degradation, surface reconstruction, and parasitic side reactions may drive cells along distinct ageing pathways, leading to the divergence observed after approximately Round 30. This behavior is consistent with the stochastic ageing framework proposed in the present study and reported previously for Ni–rich cathode systems [8].

Initial capacities are similar at approximately 57 Ah. Divergence appears during mid-life cycling. By Round 30, Cell 1 has reached 48.45 Ah, lower than Cells 2 and 3, which remain near 50 Ah. This gap persists and widens. Cell 1 shows the largest capacity fade (20.94%), and Cell 3 shows the smallest (16.02%), Table 1. The cell with the highest early-cycle deviation also ends with the poorest long-term performance. Early differences are reflected in later ageing behavior. A moderate negative correlation ($r \approx -0.50$) is observed between early-cycle deviation and final capacity, indicating that cells with larger initial deviations tend to exhibit greater long-term capacity loss.

Table 1: Degradation behavior of the three cells

Cell	Initial capacity (Ah)	Capacity at round 30 (Ah)	Final capacity (Ah)	Capacity fade (%)	Early deviation (Ah)	Relative rank
Cell 1	57.43	48.45	45.40	20.94	0.152	3 (Worst)
Cell 2	57.07	50.07	47.42	16.91	0.083	2
Cell 3	57.02	50.00	47.88	16.02	0.139	1 (Best)

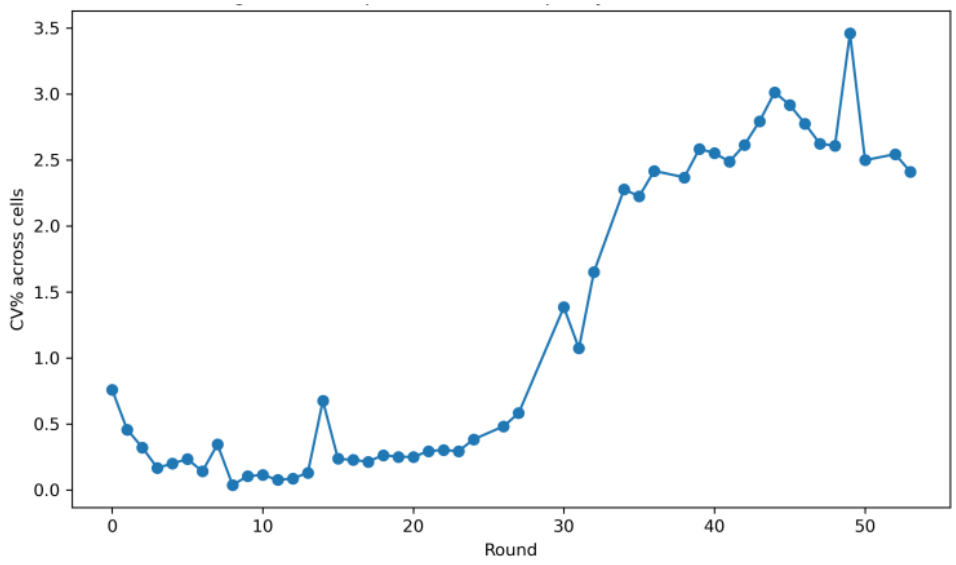

Figure 3: Cell–to–cell variability in discharge capacity (CV%) as a function of ageing round. Variability remains low during early cycles and increases after mid-life.

4.3 Lifetime dispersion

Figure 3 illustrates how cell–to–cell variability in discharge capacity-measured as the coefficient of variation (CV%), evolves with ageing rounds. During early cycles, variability stays low, generally below 1%. The cells show similar behaviour during early cycles. Significant change in the CV appears after 25 cycles, which exceeds 3% by the later stages (Table 2). The increase accelerates during mid-

life, indicating that initially small differences between cells become amplified with continued cycling. Similar behaviour is reported for Ni–rich cathodes, where local heterogeneities and stochastic processes influence degradation [8].

Table 2: Coefficient of variation (CV%) in early and late ageing stages. The results show an order-of-magnitude rise in variability from the early to the late ageing stages

Ageing interval	Coefficient of variation (CV%)
Rounds 1–10	0.25
Rounds 40–50	2.54
Overall change	∼10× increase

4.4 Diffusion-limited benchmark

A diffusion-based reference model (Equation (7)) was fitted to the experimental capacity data to assess transport-limited behavior. It does not represent a specific coated system [10, 11]. The model produces smoother capacity trajectories than the experimental data, particularly for Cells 2 and 3 (Figure 4). Its effect on variability is not uniform across the ageing process. During early cycles, dispersion remains close to the experimental case. At later stages, variability decreases modestly. The average CV decreases from approximately 2.54% to 2.20%, a reduction of about 13%. Transport–limited behavior reduces variability but does not eliminate it. Differences between cells persist, indicating continued influence of initial heterogeneity and localized degradation [8]. Together with Sections 4.2 and 4.3, the results indicate a two-stage pattern. Early divergence is associated with heterogeneous reactions, while transport effects become more noticeable at later stages and reduce the spread between cells.

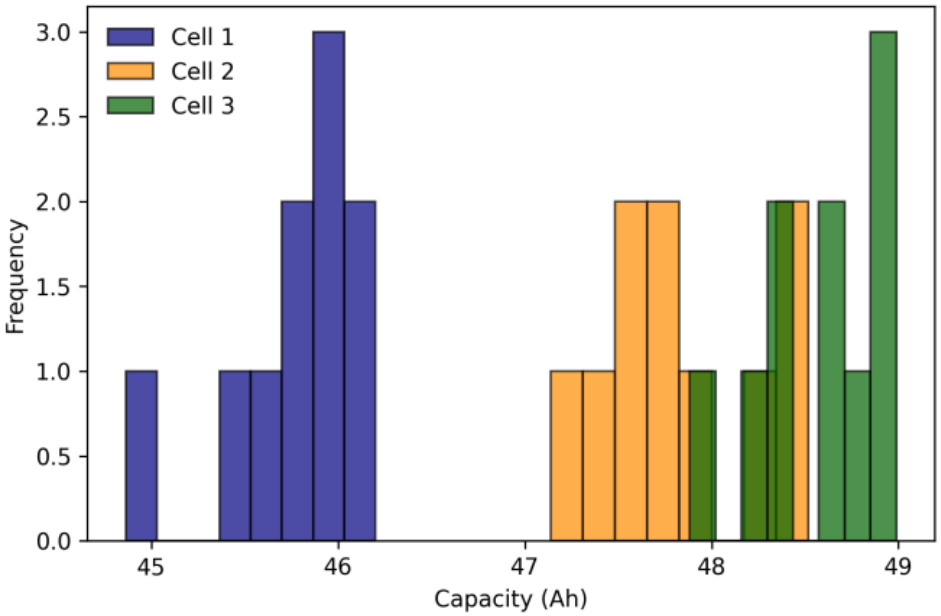

Figure 4: Discharge capacity distribution for Cells 1–3 during late-stage ageing (Rounds 40–50). Each cell forms a distinct cluster, with separation between cells larger than within-cell fluctuations.

4.5 Validation using the Severson fast-charging dataset

The Severson et al. dataset constitutes a subset of 46 commercial lithium-ion cells cycled under controlled fast-charging conditions, with per-cycle metrics such as discharge capacity, temperature, and lifetime [16]. Reported capacities ($\sim 1.0 - 1.1$ Ah initial) are internally consistent, and no scaling correction was applied. A Pearson correlation analysis between early-cycle deviation and final capacity yields a weak negative relationship ($r \approx -0.16, p > 0.05$), which suggests that early deviations do not strongly predict long-term capacity outcomes across the larger population.

Using the same analysis pipeline, the coefficient of variation (CV%) increases from $\sim$ 0.70% in early cycles to $\sim$ 3.71% at later stages ($\sim$ 5.3×amplification). The diffusion-limited $\sqrt{r}$

benchmark reduces late-stage variability to ∼ 2.30% (∼ 38% reduction). Corresponding values for the Vilsen–Stroe dataset are summarized in Table 3.

Table 3: Variability evolution and diffusion-benchmark comparison across datasets

Dataset	Cells	Early CV (%)	Late CV (%)	Amplification	Late CV model (%)	Reduction (%)
Vilsen–Stroe	3	0.25	2.54	∼10×	2.20	∼13
Severson *et al.*	46	0.70	3.71	∼5.3×	2.30	∼38

Table 4: Literature benchmarking of Al-based coatings reported for NMC811 cathodes

Literature	Coating type	Key outcome
[12]	ALD Al_2O_3	Limited improvement under moderate cycling.
[11]	ALD Al_2O_3	∼10–20% retention gain under extended cycling.
[22]	Ultrathin ALD Al_2O_3	Improved capacity retention across a wide voltage range.
[23]	ALD Al_2O_3	Reduced capacity loss at high voltage.
[10]	$LiAlO_2$-type	∼17% improvement with enhanced cycling stability.

This suggests that while variability amplification is clearly observed at the population level, the relationship between early-stage divergence and individual cell outcomes is less pronounced in larger datasets.

4.6 Literature benchmarking of Al-based coatings

Experimental studies on Al-based coatings for NMC811 report performance improvements that depend on conditions; uniformity across conditions has not been demonstrated. Table 4 summarizes the key findings. Under moderate cycling, reported benefits are limited, while larger gains are observed under high–voltage or extended operation [11, 12]. Reported improvements range from marginal changes to roughly 10–20%. The diffusion-limited reference yields smoother capacity trajectories and a modest variability reduction (≈ 13%); differences between cells persist. Coatings improve stability by moderating interfacial processes, but their effect on cell–to–cell variability is condition-dependent.

4.7 Variance convergence

Figure 5 shows variability, deviation from the diffusion-limited benchmark, and early–stage behavior. The CV% does not increase smoothly and shows intermittent excursions during early and mid-life. Deviations from the diffusion-limited reference are largest at early stages and decrease with cycling, reflecting a shift from reaction–dominated behavior to increasing transport influence. Early–cycle deviation shows a weak relationship with final capacity, with larger initial divergence only loosely associated with greater long–term capacity loss. The limited sample size in the three–cell dataset prevents statistical generalization, and comparison with the Severson dataset indicates that this relationship may not be strongly preserved at a larger scale. This suggests that early-stage heterogeneity contributes to variability amplification but is not sufficient alone to predict long-term capacity outcomes across larger populations.

5 Conclusion

Ageing variability in nickel–rich NMC811 cathodes was examined using mission–profile cycling data from three nominally identical single–crystal cells. Degradation does not proceed uniformly across cells: behavior is similar during early cycles, but capacity trajectories separate with continued cycling, and small early differences influence later ageing. A diffusion-limited $\sqrt{r}$ reference model was used to represent transport–controlled ageing. The model produces smoother capacity trends and a modest reduction in variability, but differences between cells persist as transport effects become more dominant. The behavior reflects the combined influence of interfacial reactions, mechanical degradation, and stochastic effects. The small number of cells limits statistical generalization, but early–cycle variability provides information on long–term divergence. Further work with larger datasets and coated systems is required to assess how general this behaviour is and its dependence on operating conditions.

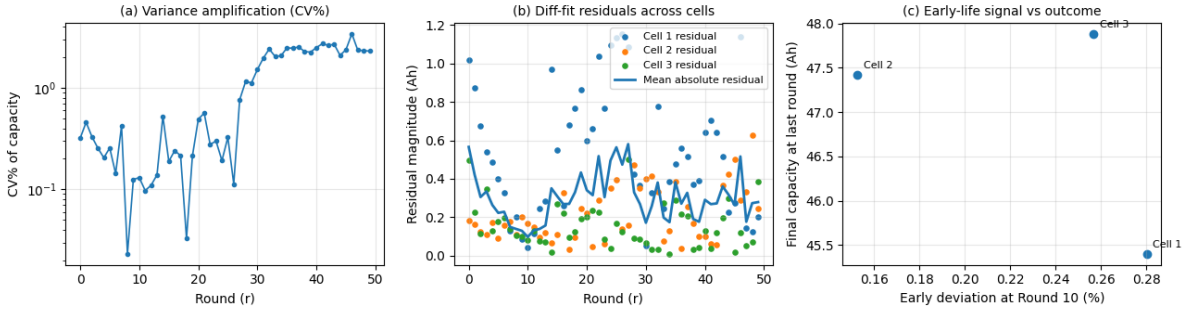

Figure 5: (a) Evolution of CV%, (b) residuals relative to the diffusion-limited model, (c) early–cycle deviation versus final capacity.

Conflict of interest

The authors declare that they have no known competing financial or personal interests.

Authors' contribution

SK: Conceptualization, research design, formal analysis, data visualization, data curation, data validation, supervision, and wrote the original manuscript. **DP:** Literature review, and critical reading of the manuscript. **AB:** Contributed to literature review, data verification and manuscript review. **PB:** Contributed to data organization, and manuscript review. **HKC:** Literature review, and manuscript review. **AP:** Contributed to data compilation, and manuscript review. **SD:** Literature review, and manuscript review. **BS:** Data organization and manuscript review.

References

[1] Gallegos-Moncayo K, Jean J, Folastre N, Jamali A, Demortiere A. Investigating cathode electrolyte interphase formation in NMC 811 primary particles through advanced 4D-STEM ACOM analysis. Symmetry. 2024;16(3):301.

[2] Iqbal N, Lee S. Anisotropic model to describe chemo-mechanical response of Ni-rich cathode materials. International Journal of Mechanical Sciences. 2024;269:109034.

[3] Omirkhan A, Gavalda-Diaz O, Wang S, Stephens IE, Giuliani F, Ryan MP. Investigating the effect of lithiation on polycrystalline NMC811 Li-ion battery cathode cracking using in situ SEM micromechanical testing. Energy and Environmental Science. 2025;18(20):9254-62.

[4] Singh MP, Kim SH, Zhou X, Kwak H, Kwiatkowski da Silva A, Antonov S, et al. Near-Atomic-Scale Evolution of the Surface Chemistry in Li [Ni, Mn, Co] O2 Cathode for Li-Ion Batteries Stored in Air. Advanced Energy and Sustainability Research. 2023;4(1):2200121.

[5] Britala L, Marinaro M, Kucinskis G. A review of the degradation mechanisms of NCM cathodes and corresponding mitigation strategies. Journal of Energy Storage. 2023;73:108875.

[6] Jaye C, Fischer DA, Quilty C, West P, Wheeler G, Housel L, et al. Elucidating Cathode Degradation Mechanisms in NMC811/Graphite Cells Under Fast Charge Rates Using Operando Synchrotron Characterization. 2022.

[7] Neudeck S, Mazilkin A, Reitz C, Hartmann P, Janek J, Brezesinski T. Effect of low-temperature Al_2O_3 ALD coating on Ni-rich layered oxide composite cathode on the long-term cycling performance of lithium-ion batteries. Scientific Reports. 2019;9(1):5328.

[8] Ogley MJW, Johnston BIJ, Hall DS, Piper LFJ. Understanding Degradation in Single-Crystalline Ni-Rich Li-Ion Battery Cathodes. Chemical Reviews. 2025;125(20):9774-806.

[9] Herzog MJ, Gauquelin N, Esken D, Verbeeck J, Janek J. Facile dry coating method of high-nickel cathode material by nanostructured Fumed alumina (Al_2O_3) improving the performance of lithium-ion batteries. Energy Technology. 2021;9(4):2100028.

[10] Riesgo-Gonzalez V, O'Keefe CA, Grey CP, Wright DS. Improving long-term capacity retention of NMC811 via lithium aluminate coatings using mixed-metal alkoxides. Journal of Materials Chemistry A. 2024;12(33):22248-61.

[11] Chen RLB, Sayed FN, Banerjee H, Temprano I, Wan J, Morris AJ, et al. Identification of the dual roles of Al_2O_3 coatings on NMC811-cathodes via theory and experiment. Energy and Environmental Science. 2025;18(4):1879-900.

[12] Huang H, Qiao L, Zhou H, Tang Y, Wahila MJ, Liu H, et al. Efficacy of atomic layer deposition of Al_2O_3 on composite LiNi0. 8Mn0. 1Co0. 1O2 electrode for Li-ion batteries. Scientific Reports. 2024;14(1):18180.

[13] Ahaliabadeh Z, Miikkulainen V, Mantymaki M, Mousavihashemi S, Lahtinen J, Lide Y, et al. Understanding the stabilizing effects of nanoscale metal oxide and Li–metal oxide coatings on lithium-ion battery positive electrode materials. ACS Applied Materials and Interfaces. 2021;13(36):42773-90.

[14] Vilsen SB, Stroe DI. Dataset of lithium-ion battery degradation based on a forklift mission profile for state-of-health estimation and lifetime prediction. Data in Brief. 2024;52:109861.

[15] Llanos PS, Ahaliabadeh Z, Miikkulainen V, Lahtinen J, Yao L, Jiang H, et al. High voltage cycling stability of LiF-coated NMC811 electrode. ACS Applied Materials and Interfaces. 2024;16(2):2216-30.

[16] Severson KA, Attia PM, Jin N, Perkins N, Jiang B, Yang Z, et al. Data-driven prediction of battery cycle life before capacity degradation. Nature Energy. 2019;4(5):383-91.

[17] Weibull W. A statistical distribution function of wide applicability. Journal of Applied Mechanics. 1951.

[18] Riesgo-Gonzalez V, Hall DS, Marker K, Slaughter J, Wright DS, Grey CP. Effect of annealing on the structure, composition, and electrochemistry of NMC811 coated with Al_2O_3 using an alkoxide precursor. Chemistry of Materials. 2022;34(21):9722-35.

[19] Faulkner LR, Bard AJ. Electrochemical methods: fundamentals and applications. Wiley; 2000.

[20] Chapra SC, Canale RP, et al. Numerical methods for engineers. vol. 1221. Mcgraw-hill New York; 2011.

[21] Newman J, Thomas-Alyea E. K. Electrochemical systems. ed: John Wiley and Sons: New York. 2004.

[22] Ahangari M, Xia F, Szalai B, Zhou M, Luo H. Advancing lithium-ion batteries' electrochemical performance: Ultrathin alumina coating on Li ($Ni_{0.8}Co_{0.1}$ $Mn_{0.1}$) O_2 cathode materials. Micromachines. 2024;15(7):894.

[23] David L, Dahlberg K, Mohanty D, Ruther RE, Huq A, Chi M, et al. Unveiling the role of Al_2O_3 in preventing surface reconstruction during high-voltage cycling of lithium-ion batteries. ACS Applied Energy Materials. 2019;2(2):1308-13.